furthermore, to a temperature dependence of the Debye temperature. For this analysis, the use of an imaging energy filter was essential.

This result is important for a general structure determination by diffraction techniques when interactions of reflections from higher-order Laue zones have to be considered. Another conclusion would be that the intentensity anomalies should be observable with a perfect crystal with atomically flat surfaces in an energy-filtered pattern.

We thank Dr K. Kambe for many discussions and for his permission to use the perturbation program. We also thank Professor A. Ichimiya for his suggestions. Mrs H. Sack-Kongehl and Mr K. Weiss are thanked for plotting the simulations, Mr J. Kühn for his help in the application of the computer equipment, and Dr A. Preusser for helping us with the complex matrix calculation.

References

ALDRED, P. J. & HART, M. (1973). *Proc. R. Soc. London Ser. A*, **332**, 223–254.
BATTERMAN, B. W. (1962). *Phys. Rev.* **127**, 686–690.
BORRMANN, G. (1941). *Phys. Z.* **42**, 157.
CROMER, D. T. & MANN, J. B. (1968). *Acta Cryst.* A**24**, 321–324.
DOYLE, P. & TURNER, A. (1968). *Acta Cryst.* A**24**, 390–397.
GOODMAN, P. (1974). *Acta Cryst.* A**28**, 92–93.
GOODMAN, P. & LEHMPFUHL, G. (1965). *Z. Naturforsch. Teil A*, **20**, 110–114.
HEIDE, H. G. (1982). *Ultramicroscopy*, **10**, 125–154.
HOLMESTAD, R., KRIVANEK, O. L., HØIER, R., MARTHINSEN, K. & SPENCE, J. C. H. (1993). *Ultramicroscopy*, **52**, 454–458.
HUMPHREYS, C. J. & HIRSCH, P. B. (1968). *Philos. Mag.* **18**, 115–122.
ICHIMIYA, A. & LEHMPFUHL, G. (1978). *Z. Naturforsch. Teil. A*, **33**, 269–281.
ICHIMIYA, A. & LEHMPFUHL, G. (1988). *Acta Cryst.* A**44**, 806–809.
ISHIDA, K., JOHNSON, A. R. & LEHMPFUHL, G. (1975). *Z. Naturforsch. Teil A*, **30**, 1715–1729.
KAMBE, K. & MOLIÈRE, K. (1970). *Advances in Structure Research by Diffraction Methods*, Vol. 3, edited by R. BRILL & R. MASON, p. 53. Oxford: Pergamon Press.
KRAHL, D. (1990). *Mater. -wiss. Werkst.* **21**, 84–90.
LAUE, M. VON (1953). *Acta Cryst.* **6**, 217–218.
LEHMPFUHL, G. & DOWELL, W. C. T. (1986). *Acta Cryst.* A**42**, 569–577.
MARADUDIN, A. A. & FLINN, P. A. (1963). *Phys. Rev.* **129**, 2529–2547.
MAYER, J., SPENCE, J. C. H. & MÖBUS, G. (1991). *Proceedings of Electron Microscopy Society of America*, edited by G. BAILEY, pp. 786–787. San Francisco Press.
MOLIÈRE, K. (1939). *Ann. Phys. (Leipzig)*, **34**, 461–472.
RACKHAM, G. M., STEEDS, J. W. & JONES, P. M. (1975). *Acta Cryst.* A**31**, S252–S253.
REIMER, L. (1989). *Transmission Electron Microscopy, Springer Series in Optical Science*, Vol. 36, p. 316. Berlin: Springer.
STEEDS, J. W. & JONES, P. M. (1975). *Acta Cryst.* A**31**, S252.
SWAMINATHAN, S., ALTYNOV, S., JONES, I. P., ZALUZEC, N. J., MAHER, D. M. & FRASER, H. L. (1994). Proc. 13th International Congress on Electron Microscopy, Paris, Vol. 1, pp. 861–862.
TANAKA, M., TERAUCHI, M. & KANEYAMA, T. (1985). *Convergent Beam Electron Diffraction*, Vols. I and II. JEOL Ltd, 1418 Nakagami, Akashima, 196 Japan.
UYEDA, R. (1968). *Acta Cryst.* A**24**, 175–181.
VOSS, R., LEHMPFUHL, G. & SMITH, P. (1980). *Z. Naturforsch. Teil A*, **35**, 973–984.
WILLIS, B. T. M. (1969). *Acta Cryst.* A**25**, 277–300.
WILLIS, B. T. M. & PRYOR, A. W. (1975). *Thermal Vibration in Crystallography*. Cambridge Univ. Press.
ZHANG, B., YANG, J., JIN, L., YE, C., BASHIR, J., BUTT, N. M., SIDDIQUE, M., ARSHED, M. & KHAN, Q. H. (1990). *Acta Cryst.* A**46**, 435–437.
ZHOU, F. (1991). Private communication.
ZHOU, F. & MÖLLENSTEDT, G. (1992). *Ultramicroscopy*, **41**, 359–366.

Acta Cryst. (1995). A**51**, 514–519

Cation Ordering Waves in Trirutiles. When X-ray Crystallography Fails?

BY STAFFAN HANSEN* AND ANGEL LANDA-CÁNOVAS

National Center for HREM, Inorganic Chemistry 2, Chemical Center, University of Lund, PO Box 124, S-221 00 Lund, Sweden

KENNY STÅHL

Inorganic Chemistry 2, Chemical Center, University of Lund, PO Box 124, S-221 00 Lund, Sweden

AND JERKER NILSSON

Chemical Technology, Chemical Center, University of Lund, PO Box 124, S-221 00 Lund, Sweden

(*Received 27 December 1994; accepted 13 March 1995*)

Abstract

Trirutiles are AB_2O_6 crystal structures with a tripled *c*-axis repeat compared to the rutile type, owing to *ABBABBA* metal ordering. Partially disordered trirutiles, space group $P4_2/mnm$, are here described by addition of a sinusoidal scattering density wave along **c** to the basic rutile structure. As a result of this approach, an infinite number of crystal structures can be envisaged, which

* To whom all correspondence should be addressed.

pairwise exhibit identical X-ray diffraction patterns, *i.e.* this is a case where the expected one-to-one relationship between crystal structure and diffraction intensity distribution is replaced by a two-to-one relationship

Introduction

A fundamental assumption in crystallography is that once a well refined crystal structure has been established there is no need to consider the possibility of a different arrangement of the same atoms that produces an identical diffraction pattern, except in the case when the two crystal structures are enantiomorphic, *i.e.* mirror images of each other. Even enantiomorphic pairs can be distinguished if high-quality diffraction data are available. Nevertheless, there are reasons to question the assumption of a one-to-one relationship between structure and diffraction pattern in some cases. It was reported by Pauling & Shappell (1930) that two different arrangements of Mn atoms were compatible with the diffraction data of the cubic mineral bixbyite, Mn_2O_3, but when the O atoms were taken into account only one of the arrangements was possible. Two structures having the same list of squared structure factors exhibit identical Patterson maps and thus they are structures where the same interatomic distances occur. Such structures were called homometric by Patterson (1939). A large number of homometric pairs has been derived theoretically but no real example, except the partial bixbyite structure (Pauling & Shappell, 1930), is mentioned in a review of the subject by Buerger (1959).

More recently, it has been argued that certain types of superstructures are better described as modulated structures (Pérez-Mato, 1991; Withers, Thompson & Schmid, 1993). A modulated structure consists of a basic structure plus an occupancy and/or a displacive wave. In the general case, the phase of the modulation wave relative to the basic structure is undeterminable. When the wave is made commensurate with the basic lattice, the phase is subject to restrictions depending on the resulting symmetry. This type of commensurate modulation can give rise to homometric crystal structures. An example is the ninefold superstructure of thiourea (Tanisaka, Mashiyama & Hasebe, 1988; Zúñiga *et al.*, 1989), where the thiourea molecules are affected by a displacement wave. Two indistinguishable, but not identical, structures are possible in space group *Pnma*. In this paper, we present an example of homometry in a simple oxide structure exhibiting a commensurate compositional modulation.

The tetragonal crystal structure of rutile, TiO_2 (Vegard, 1916), is built of rows of edge-sharing TiO_6 octahedra along the z direction. These rows of octahedra are then joined together by corner sharing in the xy plane. In a study of the mineral tapiolite, $FeTa_2O_6$, Goldschmidt (1926) established the trirutile structure, which is derived from the rutile structure by ordering of the metal ions in the rows of edge-sharing octahedra according to the sequence ...FeTaTaFeTaTaFe..., see Fig. 1(*a*). The rutile and trirutile structures are both tetragonal and have the same symmetry, *i.e.* space group $P4_2/mnm$, and the relationship between the unit cells is $a_{\text{trirutile}} = a_{\text{rutile}}$ and $c_{\text{trirutile}} = 3c_{\text{rutile}}$.

An electron diffraction study (Landa-Cánovas, Nilsson, Hansen, Ståhl & Andersson, 1994, 1995) of the rutile-related phase $Sb_{0.9}V_{0.9}\square_{0.2}O_4$ (the square denotes a vacancy) revealed the approximate supercell $a = 2\times2^{1/2}a_{\text{rutile}}$, $c = 4c_{\text{rutile}}$ but careful observation showed that the diffraction spots were slighty off position along $\mathbf{c}^*$, which indicates an incommensurately modulated structure. We thus started to think in terms of scattering density waves affecting the metal atoms in the edge-sharing octahedral rows in rutile-type crystals, waves that can be decoupled from the basic lattice in order to give an incommensurately modulated structure.

Trirutile as commensurately modulated rutile

The structural parameters of trirutile are presented in Table 1. The parameters, taken from a single-crystal neutron diffraction study of tapiolite, $FeTa_2O_6$ (von Heidenstam, 1968), have been slightly idealized so that all x coordinates of O atoms are equal, the non-zero z coordinates are exactly 1/3, the temperature factors of the two metal atoms are the same and so are the temperature factors of the two O atoms. It turns out that all fully ordered AB_2O_6 trirutiles can simply be described as commensurately modulated by a scattering density wave of the form

$$f(z) = \langle f \rangle - (2/3)g\Delta f\cos(2\pi z), \qquad (1)$$

where $f(z)$ is the scattering power in position 0,0,z along the c axis; $\langle f \rangle$ is the average scattering power equal to $(f_A + 2f_B)/3$, with f_A and f_B being the scattering factors of atom A and atom B, respectively; g is the fractional amplitude, here $g = 1$; and $f = f_B - f_A$. Note that an identical, though out-of-phase, wave is generated by symmetry along 1/2,1/2,z in the unit cell and this is implicit in the following discussion.

The continuous function along [00z] is depicted as curve (i) in Fig. 1(*b*) but it is sampled only at the cation sites, where it assumes the following values in the row of octahedra: $f(0) = f_A$ and $f(1/3) = f(2/3) = f_B$ (equivalent by symmetry). It is immediately obvious that the wave of maximum amplitude that it is possible to release from the basic lattice, *i.e.* a wave confined between f_A and f_B, is the half-amplitude wave with $g = 0.5$ drawn as curve (ii) in Fig. 1(*b*). At the cation sites along a row, this wave (corresponding to a partially disordered trirutile) assumes the following values of scattering power: $f(0) = (2f_A + f_B)/3$ and $f(1/3) =$

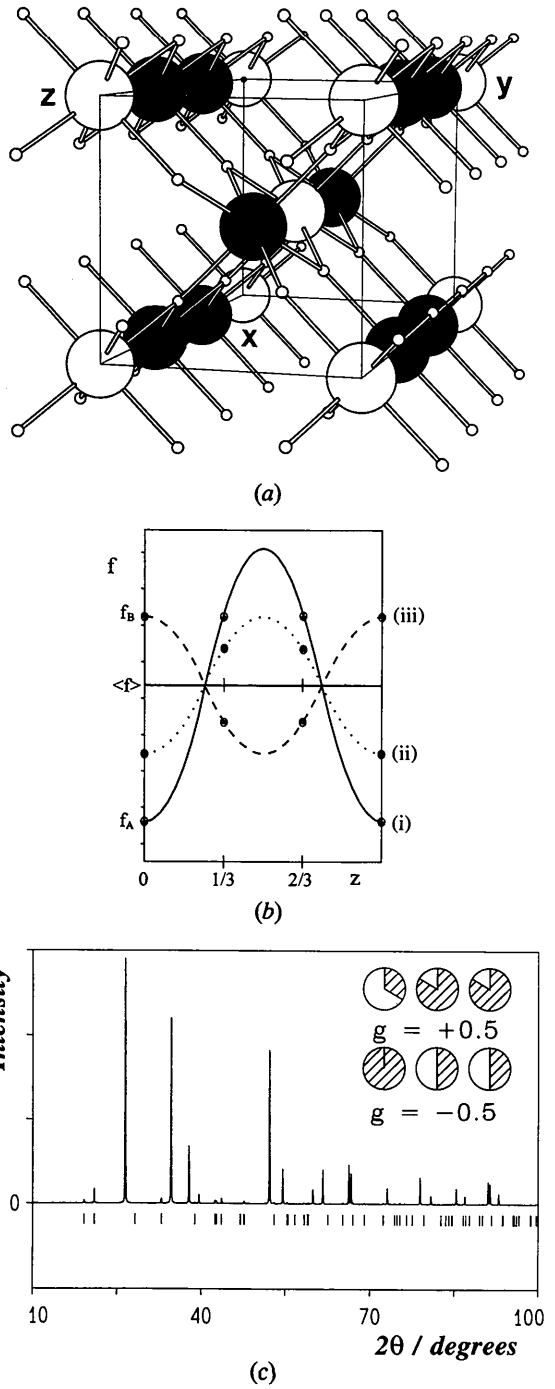

Fig. 1. (*a*) The crystal structure of trirutile AB_2O_6. Cations are drawn as large spheres (*A* atoms light and *B* atoms dark) and oxide ions as small spheres. The unit cell is outlined. (*b*) Scattering power (f) as a function of z coordinate for a scattering density wave affecting the metal positions along [00z] in the trirutile structure. (i) Full-amplitude wave, (ii) half-amplitude wave and (iii) out-of-phase wave of half-amplitude. (*c*) Calculated X-ray powder pattern for partially disordered $FeTa_2O_6$. Identical patterns are obtained for two cation distributions as illustrated by pie charts; in this case: $g = +0.5$ in equation (1); 66.7% Fe, 33.3% Ta in 2(*a*) and 16.7% Fe, 83.3% Ta in 4(*e*); and $g = -0.5$; 0% Fe, 100% Ta in 2(*a*) and 50% Fe, 50% Ta in 4(*e*). Superlattice reflections are indicated by vertical bars.

Table 1. *Idealized trirutile structure, AB_2O_6, space group $P4_2/mnm$*

	Wyckoff position*	x	y	z	B (Å^2)
A	2(*a*)	0	0	0	1.0
B	4(*e*)	0	0	1/3	1.0
O(1)	4(*f*)	0.30	0.30	0	0.9
O(2)	8(*j*)	0.30	0.30	1/3	0.9

* 2(*a*) 0,0,0; 1/2,1/2,1/2; 4(*e*) ±(0,0,z; 1/2,1/2,1/2+z); 4(*f*) ±(x,x,0; 1/2+x,1/2−x,1/2); 8(*j*) ±(x,x,z; −x,−x,z; 1/2+x,1/2−x, 1/2+z; 1/2−x,1/2+x,1/2+z).

$f(2/3) = (f_A + 5f_B)/6$. If the constant g is instead put equal to −0.5, a reversed-phase half-amplitude wave is obtained, see curve (iii) in Fig. 1(*b*), and the following scattering factors are observed: $f(0) = f_B$ and $f(1/3) = f(2/3) = (f_A + f_B)/2$.

The diffraction patterns calculated for the two structures, using the slightly idealized positional coordinates and temperature factors in Table 1 and the occupancies obtained with $g = \pm 0.5$ in (1), are identical; see the powder diffraction spectrum in Fig. 1(*c*). This, somewhat surprising, result can be rationalized by inspection of the conventional Fourier sum used to calculate the structure factors F_{hkl} for the pair of cation-ordered rutiles. The reflections *hkl* can be divided into three groups: (i) those extinguished by symmetry; (ii) the main reflections, *i.e.* those that are common to both the rutile and the trirutile structures; and (iii) the superlattice reflections that occur only in trirutile. The main and superlattice reflections are both subdivided into two categories, *a* and *b*, owing to the body-centered arrangement of the metal atoms. If the Debye–Waller factors are neglected, the following structure factors F are observed for the five resulting categories:

(i) symmetry-extinct reflections, 0*kl*: $k + l = 2n + 1$ (n integer) and *h*0*l*: $h + l = 2n + 1$ with $F = 0$;

(ii*a*) main reflections with even index sums ($l = 3n$ and $h + k + l = 2n$), with $F = 6\langle f\rangle + \Sigma_{\text{oxygens}}$, where Σ_{oxygens} is the contribution from the 12 O atoms in the unit cell;

(ii*b*) main reflections with odd index sums ($l = 3n$ and $h + k + l = 2n + 1$) with $F = \Sigma_{\text{oxygens}}$;

(iii*a*) superlattice reflections with even index sums ($l \neq 3n$ and $h + k + l = 2n$) with $F = -2g\Delta f$;

(iii*b*) superlattice reflections with odd index sums ($l \neq 3n$ and $h + k + l = 2n + 1$) with $F = 0$.

The metal ordering is manifested only in superlattice reflections with even index sums, category (iii*a*), where the structure factor is proportional to the amplitude of the wave and thus the intensity is proportional to $F^2 = 4g^2\Delta f^2$ for both $g < 0$ and $g > 0$. Since the other four categories of reflection depend only on *hkl* and not on g, all pairs of structures with $g = \pm x$ and $-0.5 \leq g \leq 0.5$ have identical intensities F^2. Thus, there is in fact an infinite number of such structure pairs.

X-ray diffraction studies of $FeTa_2O_6$ and $FeNb_2O_6$

An example of this type of fundamental ambiguity has been observed experimentally, though it was not interpreted as such. The structure of the mineral tapiolite, $FeTa_2O_6$, was carefully reinvestigated by von Heidenstam (1968) using single-crystal neutron and X-ray diffraction and it was observed that the cations were partially disordered. In the X-ray study of the cation disorder, the proportion of Ta in position 2(*e*) was varied in steps from 0 to 100% [the occupancy of 4(*e*) is then fixed by stoichiometry, see Table 1]. The residual index *R* exhibited two minima of 0.08 and, while the calculations gave no indication as to which of the two models was the correct one, von Heidenstam (1968) favored the alternative that was intermediate between two known structures, *i.e.* perfectly ordered trirutile, with 0% Ta in 2(*a*), and completely disordered trirutile, *i.e.* rutile, with 67% Ta in 2(*a*).

In order to obtain a complete set of parameters for both models, we have re-refined the tapiolite structure using the single-crystal X-ray data collected by von Heidenstam (1966), see Tables 2 and 3.* The refined models I and II are very close to the ideal structure, which exhibits identical *x* coordinates for the O atoms, variable *z* coordinates equal to 1/3 and equal temperature coefficients for the metal and O atoms, respectively. The maximum deviation between the ideal and observed structures corresponds to 6 e.s.d.s. The metal occupancy factors of model I in Table 3 correspond to 51% Fe, 49% Ta in 2(*a*) and 24%Fe, 76% Ta in 4(*e*), while the values for model II correspond to 16% Fe, 84% Ta in 2(*a*) and 42% Fe, 58% Ta in 4(*e*). These two cation distributions are almost identical to the ones calculated by putting $g = 0.25$ in (1), *i.e.* 50% Fe, 50% Ta in 2(*a*) and 25% Fe, 75% Ta in 4(*e*), while $g = -0.25$ gives 17% Fe, 83% Ta in 2(*a*) and 42% Fe, 58% Ta in 4(*e*). A random distribution of cations in trirutile, *i.e.* ordinary rutile, corresponds to $g = 0$ and 33.3% Fe and 66.7% Ta in both sites. We have thus confirmed the conclusion (von Heidenstam, 1968) that least-squares refinements cannot distinguish between the two models, using the present X-ray data set, and we have explained the basic reason for this by showing that the models represent two commensurate sinusoidal scattering density waves along [00*z*] that are fully out of phase with each other.

Which of the two structures emerges in the calculations above will only depend on the starting point of the refinement. This is bad enough but it turns out that the same goes for the bond distances. Inspection of the average metal–oxygen distance in each octahedron along [00*z*] reveals the octahedron-size sequence big–small–small for model I and small–big–big for model II. Although the difference between 'big' and 'small' is only 3–4 standard deviations, the tendency is clear. The expected distances have been calculated using the bond-valence expression of Brown & Altermatt (1985) and ideal bond valences of 2/6 for Fe^{2+}—O and 5/6 for Ta^{5+}—O. The predicted metal–oxygen distances were 2.140 Å for Fe^{2+} and 1.987 Å for Ta^{5+}, and the metal–oxygen distance in octahedra with mixed metal occupancy was then simply calculated as a linear combination of the two extreme values determined by the composition. As can be seen in Table 3, the predicted distances are within 0.01 Å of those observed in the refinements of models I and II, although the bond distances are of little use when making a choice between the two models since the observed bond distances are completely model dependent.

Also of interest in the present context is a single-crystal study (Aruga, Tokizaki, Nakai & Sugitani, 1985) of synthetic $FeNb_2O_6$, performed in a space group of lower symmetry ($P\bar{4}2_1m$), where the three metal positions become crystallographically independent, which

Table 2. *Crystal data for tapiolite from von Heidenstam (1968)*

Formula	$FeTa_{0.8}Nb_{0.2}O_6$
Crystal system	Tetragonal
Space group	$P4_2/mnm$
Z	2
a (Å)	4.7515 (3)
c (Å)	9.254 (1)

Table 3. *Re-refined crystal structures of tapiolite,* $FeTa_2O_6$, *occupancy factors (n), positional coordinates (x, z), isotropic temperature coefficients (B), residual indices R(F) and average metal–oxygen distance* ⟨*M*—O⟩ *in octahedra [predicted values in brackets]*

Position		Model I	Random	Model II
2(*a*)	*n*(Fe)	0.064 (1)	0.042	0.020 (1)
	n(Ta)	0.061*	0.083	0.105*
	B (Å²)	0.93 (9)	1.0 (2)	1.14 (7)
4(*e*)	*n*(Fe)	0.061*	0.083	0.105*
	n(Ta)	0.189*	0.167	0.145*
	z	0.3327 (1)	1/3	0.3341 (2)
	B (Å²)	1.09 (6)	1.0*	0.99 (8)
4(*f*)	*x*(O)	0.312 (4)	0.310 (8)	0.306 (4)
	B (Å²)	1.2 (4)	1.5 (8)	1.8 (4)
8(*j*)	*x*(O)	0.308 (3)	0.310*	0.311 (3)
	z(O)	0.330 (2)	1/3	0.336 (2)
	B (Å²)	1.6 (3)	1.5*	1.3 (3)
	R(*F*)	0.076	0.136	0.076
2(*a*)	⟨*M*—O⟩ (Å)	2.05 (1)† [2.06]	2.03 (3)† [2.04]	2.00 (1)† [2.00]
4(*e*)	⟨*M*—O⟩ (Å)	2.02 (1)‡ [2.02]	2.03 (3)† [2.04]	2.04 (1)‡ [2.05]

* Coupled parameter.
† $\langle\sigma\rangle = 1/6[(4\sigma_1)^2 + (2\sigma_2)^2]^{1/2}$.
‡ $\langle\sigma\rangle = 1/6[(2\sigma_1)^2 + (2\sigma_2)^2 + (2\sigma_3)^2]^{1/2}$.

* Observed structure factors compared with those from a random model and models I and II have been deposited with the IUCr (Reference: AB0338). Copies may be obtained through The Managing Editor, International Union of Crystallography, 5 Abbey Square, Chester CH1 2HU, England.

reported the refined occupancies 18% Fe, 82% Nb/43% Fe, 57% Nb/39% Fe, 61% Nb. This is again very close to the sinusoidal wave expected for $g = -0.25$ in (1). The expected distance Nb^{5+}—O is 1.978 Å, which is not very different from the distance Ta—O calculated previously. The observed average distances Nb—O in the octahedra are [predicted distances in brackets]: 2.01 [2.00], 2.05 [2.04], 2.04 Å [2.05 Å] (small, big, big), as expected compared to $FeTa_2O_6$. The discussion above suggests that further work is needed in order to determine if the deviations in the positional parameters, between the ideal structure and the real ones, are big enough to resolve the outlined structural problem by X-ray methods.

Recently, two different structure models for a sphalerite-related superstructure in the Ni–Si–P system has been refined to R values below 2.5% using the same single-crystal X-ray data set (Wallinda & Jeitschko, 1995). The reason for this interesting observation is that the structure of composition $NiSi_2P_3$ corresponds to a scattering density wave of the type that is generated by putting $g = +1$ in (1), while the structure of composition $Ni_{1.28}Si_{1.28}P_3$ corresponds to a wave with $g = -1$.

High-resolution electron microscopy of $(Sb,Al,V)_3O_6$

We have observed a trirutile-like structure with a decoupled scattering density wave in the phase $(Sb,Al,V)_3O_6$ using electron diffraction, see Fig. 2(*a*). This phase has interesting catalytic properties and alumina-supported antimony vanadium oxide catalysts can be used for the ammoxidation of propane to form acrylonitrile. When aluminium antimonate is doped with vanadium, a catalyst selective for the formation of acrylonitrile is obtained (Andersson, Andersson, Centi, Graselli, Sanati & Trifirò, 1993). The diffraction patterns of $(Sb,Al,V)_3O_6$ are similar to those of a trirutile, except for the facts that the superlattice reflections are often clearly incommensurate with the basic lattice in the c^* direction and the appearence of weak reflections like 010 and 003. Modulation wavelengths in the interval $2.7–3.2c_{rutile}$ have been observed, though the crystal in Fig. 2(*a*) is very close to commensurate, with a measured wavelength of $3.0c_{rutile}$. The amplitude of the wave is small, since the superlattice reflections are not observed by Guinier X-ray powder diffraction but only by electron diffraction where the dynamical contribution to the diffraction enhances the weak superlattice spots and the signal-to-noise ratio is better. The observed 010 and 003 reflections break the *n*-glide symmetry of space group $P4_2/mnm$. The compositional wave in (1) is compatible with this symmetry and $g = \pm x$ corresponds to a modulation wave with phase 0 or 180°. If the phase assumes other values, the symmetry is automatically lowered. Further decrease in symmetry leads to the observed appearance of forbidden reflections. Similar arguments can probably also be applied to the previously mentioned $FeNb_2O_6$ structure.

Modulation theory (Korekawa, 1967) allows the following observations to be made on $(Sb,Al,V)_3O_6$: (i) the type of satellite reflections present does not vary with scattering angle, which is typical for a scattering density modulation (as opposed to a displacement modulation, where the type of satellite spots present is strongly scattering-angle dependent); (ii) only first-order satellites are observed, which is compatible with a sinusoidal wave (as opposed to a square wave, which gives appreciable intensity in satellites of higher orders).

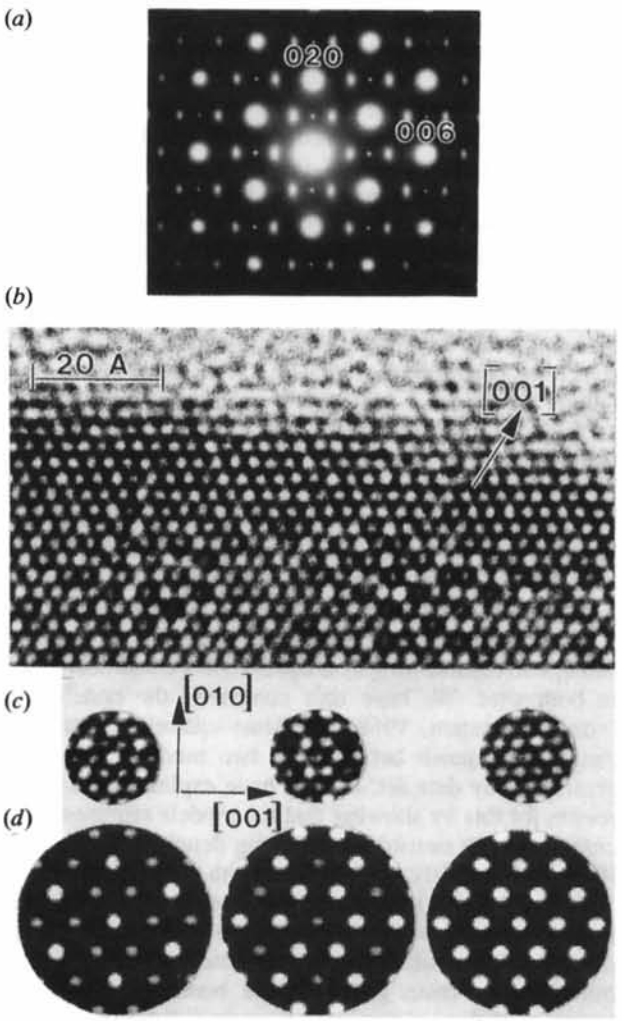

Fig. 2. (*a*) Electron diffraction pattern of an $(Sb,Al,V)_3O_6$ crystal recorded with the *a* axis parallel to the electron beam. (*b*) Atomic resolution image of the same crystal, with light spots corresponding to metal-atom positions. (*c*) Areas selected from the left part of (*b*), showing different types of local cation ordering. (*d*) Calculated images: left $g = -0.5$ or heavy–light–light atom ordering along **c** in the horizontal direction; middle $g = +0.5$ or light–heavy–heavy atom ordering; right $g = 0$ or random trirutile, *i.e.* rutile.

High-resolution electron microscopy should in principle be able to solve the problem of deciding between the two models with $g = \pm x$, since the phase information is preserved in the experiment. High-resolution images of $(Sb,Al,V)_3O_6$ exhibit soft contrast variations overlaying the basic lattice fringes, typical for density-modulated crystal structures. It turns out that the cation modulation can be studied at atomic resolution, see Fig. 2(*b*). This is most clear in the lower part of the image, where different types of ordering at the unit-cell level can be observed. In order to make the ordering clearer, three slightly overlapping areas, at the same distance from the edge of the crystal, have been selected in Fig. 2(*c*). Since the three areas selected can be assumed to possess the same thickness along the electron beam and the focus is the same for the whole image, the three areas are directly comparable. In Fig. 2(*d*), images have been simulated for out-of-phase ordering ($g < 0$), normal ordering ($g > 0$) and complete disorder ($g = 0$) and these are similar to the corresponding experimental images. Inspection of the image in Fig. 2(*b*) thus reveals that all three types of cation ordering occur side by side at the unit-cell level. It thus seems to be possible to study how the continuous scattering density wave in this type of material is actually accommodated by a set of atoms with discrete values of scattering power.

Experimental details for $(Sb,Al,V)_3O_6$

High-resolution imaging: transmission electron microscope JEM-4000EX, acceleration voltage 400 kV, structural resolution 1.6 Å, spherical aberration 1.0 mm, through-focus series recorded in steps of 100 Å. Image simulations: multislice method using computer program *NCEMSS* (Kilaas, 1987) on VAX station, composition used $AlSb_2O_6$, space group $P4_2/mnm$, crystal thickness 46 Å, defocus −600 Å, objective aperture 0.6 $Å^{-1}$. Unit cell: $a = 4.5221\,(3)$, $c = 3 \times 2.9761\,(5)$ Å, powder X-ray data, Guinier camera, Cu $K\alpha_1$ radiation, Si standard. Energy-dispersive X-ray microanalysis: $Sb_{1.5(1)}Al_{1.1(1)}V_{0.4(1)}O_6$, Link AN10000 system on scanning electron microscope JSM-840A, acceleration voltage 20 kV, point analysis of ten crystals, ZAF correction applied. Preparation: finely ground Sb_2O_3, $Al(OH)_3$ and V_2O_5 in molar ratio 1:1:0.5, heated in air at 1273 K for 4 d. Both Sb and V oxides are lost to the atmosphere during synthesis.

We want to express our gratitude to the Swedish Natural Science Research Council (SH and KS), the Ministerio Español de Educación y Ciencia (ALC) and the Swedish Research Council for Engineering Sciences (JN) for financial support.

References

ANDERSSON, A., ANDERSSON, S. L. T., CENTI, G., GRASELLI, R. K., SANATI, M. & TRIFIRÒ, F (1993). *Proceedings of the 10th International Congress on Catalysis. Studies in Surface Science and Catalysis*, edited by L. GUSZI, F. SOLYMOSI & P. TÉTÉNYI, Vol. 75, pp. 691–705. Elsevier: Amsterdam.

ARUGA, A., TOKIZAKI, E., NAKAI, I. & SUGITANI, Y. (1985). *Acta Cryst.* C**41**, 663–665.

BROWN, I. D. & ALTERMATT, D. (1985). *Acta Cryst.* B**41**, 244–247.

BUERGER, M. J. (1959). *Vector Space and its Application in Crystal-Structure Investigation*, pp. 41–50. New York: Wiley.

GOLDSCHMIDT, V. M. (1926). *Skr. Nor. Vidensk. Akad. Oslo*, No 1, pp. 17–19.

HEIDENSTAM, O. VON (1966). *Inorg. Phys. Chem. Data Inf. Ser.* No. 28. Univ. Stockholm, Sweden.

HEIDENSTAM, O. VON (1968). *Ark. Kemi*, Bd 28, No 23, pp. 375–387.

KILAAS, R. (1987). *Proc. Annu. Meet. Electron Microsc. Soc. Am.* **45**, 66–67.

KOREKAWA, M. (1967). Habilationsschrift. Ludwig-Maximilians-Univ., München, Germany.

LANDA-CÁNOVAS, A. R., NILSSON, J., HANSEN, S., STÅHL, K. & ANDERSSON, A. (1994). *Proceedings of the 13th International Congress on Electron Microscopy. Electron Microscopy* 1994, edited by B. JOUFFREY & C. COLLIEX, Vol. 3B, pp. 873–874. Paris: Les Editions de Physique.

LANDA-CÁNOVAS, A. R., NILSSON, J., HANSEN, S., STÅHL, K. & ANDERSSON, A. (1995). *J. Solid State Chem.* In the press.

PATTERSON, A. L. (1939). *Nature (London)*, **143**, 939–940.

PAULING, L. & SHAPPELL, M. D. (1930). *Z. Kristallogr.* **75**, 128–142.

PÉREZ-MATO, J. M. (1991). *Methods of Structural Analysis of Modulated Structures and Quasicrystals*, edited by J. M. PÉREZ-MATO, F. J. ZÚÑIGA & G. MADARIAGA, pp. 117–128. Singapore: World Scientific.

TANISAKI, S., MASHIYAMA, H. & HASEBE, K. (1988). *Acta Cryst.* B**44**, 441–445.

VEGARD, L. (1916). *Philos. Mag.* **32**, 65–96.

WALLINDA, J. & JEITSCHKO, W. (1995). *J. Solid State Chem.* **114**, 476–480.

WITHERS, R. L., THOMPSON, J. G. & SCHMID, S. (1993). *Acta Cryst.* A**49**, C334.

ZÚÑIGA, F. J., MADARIAGA, G., PACIOREK, W. A., PÉREZ-MATO, J. M., EZPELETA, J. M. & ETXEBARRIA, I. (1989). *Acta Cryst.* B**45**, 566–576.